

Article

Effect of Nano-Ti Particles on Microstructure and Mechanical Properties of Mg-3Al-1Zn Matrix Composites

Wei Tian ^{1,2,*} , Pengfei Gao ¹, Shengli Han ^{3,*}, Xiaohong Chen ⁴, Fuwei Zhang ¹, Yuhui Zhang ³, Tiegang Luo ³ and Kaihong Zheng ³

¹ School of Science, University of Shanghai for Science and Technology, Shanghai 200093, China

² Co-Innovation Center for Energy Therapy of Tumors, Shanghai 200093, China

³ Guangdong Key Laboratory of Metal Strengthening and Toughening Technology and Application, Institute of New Materials, Guangdong Academy of Sciences, National Titanium and Rare Metal Powder Metallurgy Engineering Technology Research Center, Guangzhou 510651, China

⁴ School of Materials and Chemistry, University of Shanghai for Science and Technology, Shanghai 200093, China

* Correspondence: tianweisst@163.com (W.T.); hanshengli@gdinm.com (S.H.)

Abstract: In this paper, a new nanoscale metal Ti particle-reinforced Mg-3Al-1Zn matrix composite was successfully designed and prepared, which is mainly characterized by the fact that in addition to the “light” advantages of magnesium matrix composite, it also realizes bidirectional improvement of strength and ductility of the composite, and can be used as an alternative material for military light vehicle armor and individual armor. The SEM test shows that the nano-Ti particles are uniformly distributed at the grain boundary under the extruded state, which nails the grain boundary, inhibits the grain growth, and significantly refines the grain. XRD tests show that the addition of nano-Ti particles increases the crystallinity of the composite, which is consistent with the SEM test results. In addition, the EBSD test shows that the weakening of the texture of Ti/Mg-3Al-1Zn matrix composites and the increase in the starting probability of slip system are the main reasons for the improvement in ductility. Mechanical tests show that the yield strength, tensile strength, and elongation of the 0.5 wt% Ti/Mg-3Al-1Zn matrix composites exceed the peak values of ASTM B107/B107M-13 by 38.6%, 26.7%, and 20%, respectively.

Keywords: nano-Ti; Mg-3Al-1Zn matrix composite; strength; ductility; bidirectional improvement



Citation: Tian, W.; Gao, P.; Han, S.; Chen, X.; Zhang, F.; Zhang, Y.; Luo, T.; Zheng, K. Effect of Nano-Ti Particles on Microstructure and Mechanical Properties of Mg-3Al-1Zn Matrix Composites. *Materials* **2023**, *16*, 2407. <https://doi.org/10.3390/ma16062407>

Academic Editor: Bolv Xiao

Received: 18 February 2023

Revised: 13 March 2023

Accepted: 16 March 2023

Published: 17 March 2023



Copyright: © 2023 by the authors. Licensee MDPI, Basel, Switzerland. This article is an open access article distributed under the terms and conditions of the Creative Commons Attribution (CC BY) license (<https://creativecommons.org/licenses/by/4.0/>).

1. Introduction

With the characteristics of mobility and flexibility, light armored vehicles undertake important tasks such as reconnaissance, command, and rescue in the complex battlefield environment [1], and the selection of their armored materials is mainly based on low density, high strength, and high ductility [2,3]. It is well known that magnesium has a low density [4], and Mehara’s research shows that the average density of medium-strength magnesium alloy is 1.78 g/cm³, which is converted into a specific strength roughly equivalent to 5083 aluminum armored alloy [5]. However, because magnesium matrix composites have a lower density than aluminum armor alloys, they are expected to become an alternative material for military light vehicle armor and individual armor.

However, the bottleneck of traditional magnesium matrix composite research is the mutual constraint of strength and ductility [6–8]. Therefore, the focus of future research on magnesium matrix composites should be around the bidirectional improvement of strength and ductility. The strength of the material is the primary factor in judging whether the material performance of military light armor is excellent, and the addition of appropriate particle reinforcement during preparation is one of the effective ways to improve the strength of the material [9–13]. Traditional reinforcing particles are ceramic particles such as silicon carbide [14], alumina [15], boron carbide [16], and TiC [17]. Yang’s [18] study

showed that the strength improvement of magnesium matrix composites mainly depended on the addition of reinforced particles to significantly refine grains. Wu [19] prepared SiC/AZ61 magnesium matrix composite, and the addition of SiC particles limited the growth of dynamic recrystallization grains, so that the grains were refined, and the tensile strength of the composite reached 386 MPa, while the elongation was only 4.7%. Peng [20] prepared TiB₂/AZ31 magnesium matrix composites with TiB₂ particles as reinforcement, and the tensile strength of the composite reached 237 MPa, but the elongation was only 4.6%. Habibnejad [21] prepared Al₂O₃/AZ31 magnesium matrix composites with Al₂O₃ particles as reinforcement, and the tensile strength of the composite reached 253 MPa, but the elongation was only 3.9%. Wang [22] prepared TiC/AZ91 magnesium matrix composites with TiC particles as reinforcements, and the strength of the composites was greatly improved, but the elongation was only 1.5%. It can be seen that although the addition of ceramic particles improves the strength of magnesium matrix composites, it leads to a significant loss of elongation.

Another focus of military light armor materials is the ductility of the material. The results of Ye [23] show that good interface bonding and co-deformation between the reinforcement and the matrix were the key to the improvement in the ductility of magnesium matrix composites. Zhou [24] used carbon nanotubes as reinforcement to prepare CNTs/AZ31 magnesium matrix composites; the interface of the composite materials was well bonded and its elongation reached an amazing 14%, but its yield strength was only 215 MPa. Feng [25] used Ni particles as metal reinforcement, Ni/AZ61 magnesium matrix composites were prepared, and the tensile strength of the composite reached 284 MPa, and its elongation was slightly damaged compared with the matrix. Wong [26] used Cu particles as metal reinforcement to prepare Cu/Mg composites, and its yield strength and tensile strength reached 237 MPa and 286 MPa, respectively, and its elongation was slightly damaged compared with the matrix.

Chin [27], Ho [28], Kwasniak [29], etc., show that the addition of copper (Cu), nickel (Ni), molybdenum (Mo) and titanium (Ti) can effectively improve the strength and ductility of the composite material [25–34]. However, Cu and Ni form intermetallic compounds Mg₂Cu [35] and Mg₂Ni [36] with Mg, which hinder the ductility of magnesium-based composites [28,35,36]. There is no interface reaction between Mo and Mg matrix [23], but its wettability with Mg and its grain refinement effect have not been widely reported. It is difficult for Ti and Mg to react with Mg to form hard or nondeformable intermetallic compounds in various metal reinforcements [37–39], and Ti and Mg have similar crystal structures at room temperature, which favors the interfacial binding of Ti and Mg [40,41]. In addition, Ti has good ductility [42–45], and during the deformation process, Ti will co-deform with the Mg matrix, which helps to improve the ductility of the composite. Therefore, metal Ti particles should be ideal reinforcements for the preparation of magnesium-enhanced matrix composites of metal particles.

Studies by Dieringa [30], Sankaranarayanan [46], Park [47], etc., have shown that the yield strength, tensile strength, and work hardening rate of composite materials all increase with the decrease in the particle size of the reinforcement. The decrease in particle size will lead to an increase in the strain gradient in the matrix, resulting in an increase in dislocation and an improvement in the comprehensive mechanical properties of the composite. Numerous studies have shown that the interfacial bonding between the enhancer and the Mg matrix greatly affects the final mechanical properties of the material [48–50], and increasing the contact area between the reinforcement and the matrix is obviously beneficial to the interfacial bonding [32]. Ye [23] prepared Ti/AZ31 magnesium matrix composites with micron Ti particles as reinforcements, and the addition of Ti particles realized the bidirectional improvement of the strength and ductility of the composites. Therefore, the design of nano-Ti-reinforced magnesium matrix composites on the basis of micron-scale reinforcements should be able to better achieve bidirectional improvement of strength and ductility.

In general, for powder metallurgy and stirred casting, the reinforcement has better dispersion in the composites prepared by powder metallurgy method [51,52]. However, the density of composites prepared by conventional powder metallurgy may have certain defects [53], and hot extrusion can improve this defect [54]. In this paper, a new nanoscale Ti particle-reinforced Mg-3Al-1Zn matrix composite was prepared by introducing a hot extrusion process based on powder metallurgy, which can be used as an alternative material for military lightweight armor.

2. Materials and Methods

2.1. Materials

In this work, spherical Ti powder with average size of 50–100 nm and purity of 99% (Jinna New Material Technology Co., Ltd., Foshan, China) and spherical AZ31 powder with average size of 100 µm and purity of 99.9% were used as raw material powder (see Table 1 for elemental composition).

Table 1. AZ31 magnesium alloy.

Elemental	Mg	Al	Zn	Cu, Fe, Mn, Ni, Si
Composition (%)	Remaining	2.90	0.87	<0.005

This study uses powder metallurgy method to prepare composite materials. The composition design of composite materials is based on the complete coating of matrix powder with reinforced body powder. The composition of the composite material is calculated as follows:

$$S_1 = 4\pi r^2 \quad (1)$$

$$S_2 = 4\pi R^2 \quad (2)$$

S_1 and S_2 represent the surface area of Ti particles and Mg-3Al-1Zn powder, respectively. r and R represent the radio of Ti particles and Mg-3Al-1Zn powders, respectively. When the substrate powder is completely coated, it can be concluded that:

$$S_2 = \frac{n}{2} S_1 \quad (3)$$

In formula (3), n is the number of nano Ti particles completely coated with Mg-3Al-1Zn matrix powder. Combined with Equations (1)–(3), the following can be obtained:

$$n = \frac{2R^2}{r^2} \quad (4)$$

$$M_1 = \rho_1 \frac{4}{3} \pi r^3 \quad (5)$$

$$M_2 = \rho_2 \frac{4}{3} \pi R^3 \quad (6)$$

M_1 and M_2 represents the mass of single Ti particles and single Mg-3Al-1Zn matrix powder, respectively. ρ_1 and ρ_2 are the densities of nano-Ti particles and Mg-3Al-1Zn matrix powder, respectively ($\rho_1 = 4.51 \text{ g/cm}^3$, $\rho_2 = 1.73 \text{ g/cm}^3$). By combining Equations (4)–(6), the composition ratio of the composite material in the case of complete coating can be obtained:

$$M_2 : nM_1 = \frac{R\rho_2}{2r\rho_1} \quad (7)$$

According to the powder particle size combination Formula (7) of nano-Ti and Mg-3Al-1Zn matrix, the proportion of nano-Ti is 0.26–0.58 wt%. Therefore, the composition is designed as (0, 0.5, 1) wt% to reduce the experimental error.

2.2. Fabrication of the Composite

The composites were prepared using powder metallurgy subsequent hot extrusion, and the fabrication procedure is shown in Figure 1. The powder mixer SHY-5 was used to mix 0 wt%, 0.5 wt%, and 1 wt% nano-Ti with Mg-3Al-1Zn matrix powder at room temperature for 4 h. The mixed powder was loaded into a vibration tank and transferred to a vibration table model (TM2101-17) with the vibration direction of Y axis, a frequency of 28 Hz, and vibration for 10 min under argon gas. XGB12 planetary ball mill was used for high-energy ball milling of mixed powder in argon environment with a ball-to-material ratio of 20:1 and a speed of 250 r/min for 2 h. The homogeneously mixed composite powders were compacted into a cylinder with a diameter of 20 mm and a height of 200 mm under a pressure of 600 MPa. The Ti/Mg-3Al-1Zn-based composites were sintered at a high temperature of 120 min by heating at a heating rate of 5 °C/min in argon atmosphere at 500 °C. The composites were preheated at 400 °C for 90 min and then hot-extruded (extrusion ratio 16:1) at an extrusion speed of 0.5 m/s. The density of extruded Ti/Mg-3Al-1Zn composites was measured by digital densimeter. The theoretical density and actual density of the composites are shown in Table 2.

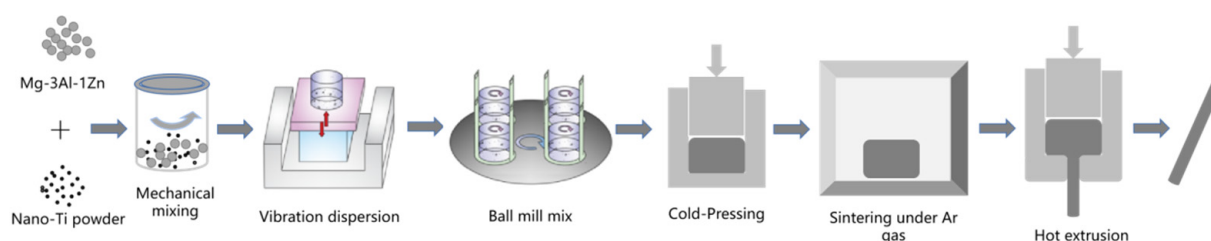


Figure 1. Schematic diagram of the fabrication procedure of Ti/Mg-3Al-1Zn composites.

Table 2. Densities of the as-extruded Ti/Mg-3Al-1Zn composites.

Composite	Theoretical Density (g/cm ³)	Actual Density (g/cm ³)
0 wt% Ti	1.7803	1.7214
0.5 wt% Ti	1.7857	1.7425
1 wt Ti	1.7808	1.7442

2.3. Characterization

The morphology of elemental powder and nano-Ti/Mg-3Al-1Zn mixed powder was observed by scanning electron microscopy (SEM FEI Nova Nano). The phase composition of the samples was determined by an advanced X-ray diffractometer (XRD Bruker D8). The scanning range was 2θ (20–90°) and the scanning speed was 2°/min. The microstructure of sintered nano-Ti/Mg-3Al-1Zn matrix composites and Mg-3Al-1Zn matrix was observed by light microscopy (OM Zeiss DM2500M 3.1MPCCD) and SEM. To observe the crystal structure, the sintered sample was etched using AC₂ reagent (Table 3), and the corresponding grain size of the extruded composite and the Mg-3Al-1Zn magnesium alloy was measured.

Table 3. Composition list of AC₂ reagents.

Component	Ethanol	Propanol	Distilled Water	Perchloric Acid	Citric Acid	Hydroxyquinoline	Sodium Thiocyanate
Content	800 mL	100 mL	18.5 mL	15 mL	75 g	10 g	41.4 g

The mechanical properties of Ti/Mg-3Al-1Zn-based composite extruded states with different mass fractions (0 wt%, 0.5 wt%, 1 wt%) were measured by performing tensile experiments at a displacement rate of 2 mm/min in the tensile testing machine (Zwiki-Z250) at room temperature. Three cylindrical samples with a diameter of 9 mm and a height of 140 mm were prepared from each component by machining for tensile test.

3. Results

3.1. Evolution of Nano-Ti/Mg-3Al-1Zn Mixed Powder during Dispersion Treatment

As shown in Figure 2a, the matrix Mg-3Al-1Zn powder used in the experiment is a regular sphere with a particle size of 100 μm . The morphology of the reinforcement nano-Ti powder is shown in Figure 2b, and the particle size of the powder is 50–100 nm. As can be seen from the figure, larger aggregates composed of multiple nano-Ti particles can be observed due to van der Waals forces and electrostatic attraction between powders [55]. Figure 3 shows the scanning images of the surface of the Ti/Mg-3Al-1Zn mixed powder with different mass fraction nanoparticles. The gray spherical particles in the figure are Mg-3Al-1Zn powders and the white bright spots are nano Ti particles, and the coating rate of the substrate surface is higher with the increase in the content. In addition, larger white bright spots can be observed in Figure 3c, which are caused by the agglomeration of nano Ti particles.

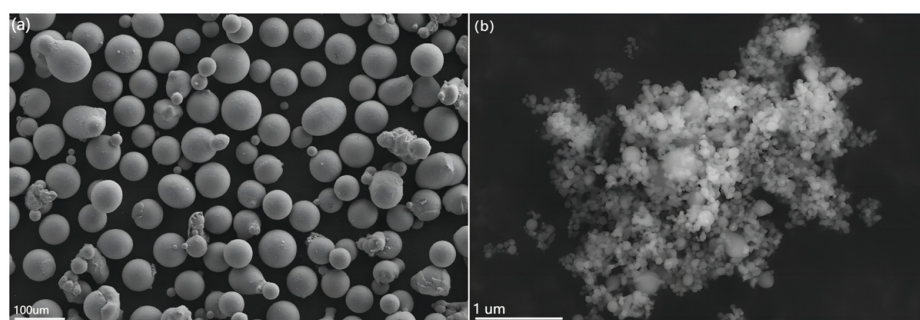


Figure 2. SEM view of the powder surface: (a) Mg-3Al-1Zn powder, (b) nano-Ti powder.

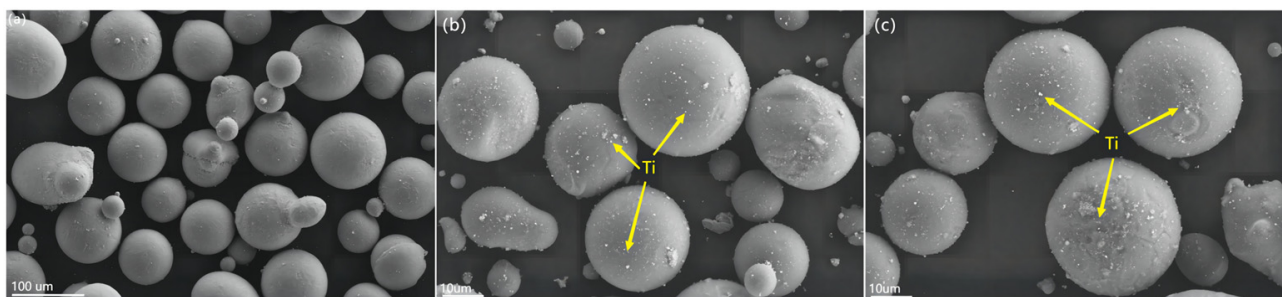


Figure 3. SEM view of the powder surface: (a) 0 wt% Ti/Mg-3Al-1Zn, (b) 0.5 wt% Ti/Mg-3Al-1Zn, (c) 1 wt% Ti/Mg-3Al-1Zn.

3.2. Microstructure of Ti/Mg-3Al-1Zn Composite

Figure 4 shows the XRD patterns of the extruded state of the composites containing (0–1) wt% Ti/Mg-3Al-1Zn matrix. The figure shows the strong peaks associated with Mg, and compared with the matrix, the Mg peak gradually increases with the increase in nano-Ti content, which indicates that the addition of Ti particles increases the crystallinity of the composite and refines the grains [56]. In addition, weak Ti peaks can be observed in the XRD plots, which are not easily detected by XRD when the content of the reinforcement in the composite is less than 5 wt%.

Figure 5 shows the OM diagram and grain size statistics of the extruded Ti/Mg-3Al-1Zn matrix composites. In the composites, most of the grains are equiaxed grains rather than deformed grains, which indicates that dynamic recrystallization (DRX) occurs in the hot extrusion process [46]. The average grain size of 0 wt% Ti composites measured by EBSD is about 6.2 μm , while the average grain size of 0.5 wt% Ti composites is 4.516 μm , which is significantly reduced by 30% compared with the matrix grain size. This indicates that the addition of nano-Ti particles makes the grain of the composite material significantly refined. This shows that during the preparation process, nano-Ti particles coated on the

surface of the matrix play a role in pinning grain boundaries and inhibiting grain growth. In addition, in the statistics of grain size, it is found that the grain size difference is large in the composites containing Ti, and the number of fine grains in the composites increases with the increase in Ti content, and the gap between grain sizes decreases gradually. However, the average grain size of 1 wt% Ti composite is 4.258 μm , which only decreases by 5% compared with that of 0.5 wt% Ti composite. This phenomenon reflects that the increase in nano Ti does not make the grain refinement of the composites continue. The uneven distribution of nano-Ti particles and the failure to cover all grains are the main reasons for the difference in grain size [57,58].

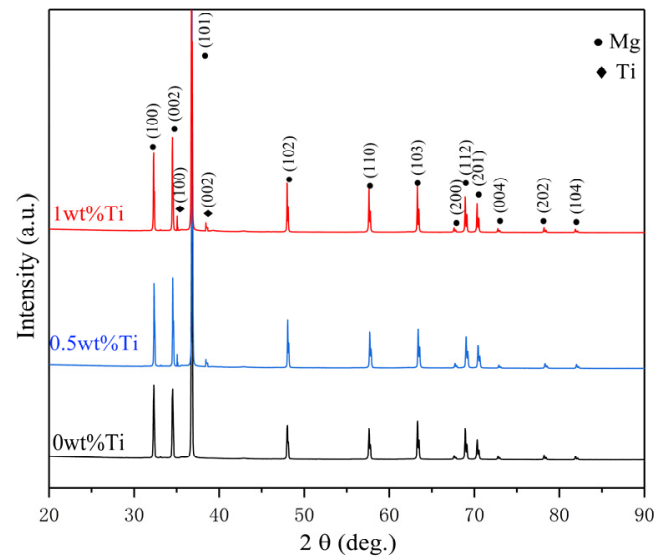


Figure 4. XRD patterns of as-extruded Ti/Mg-3Al-1Zn composites.

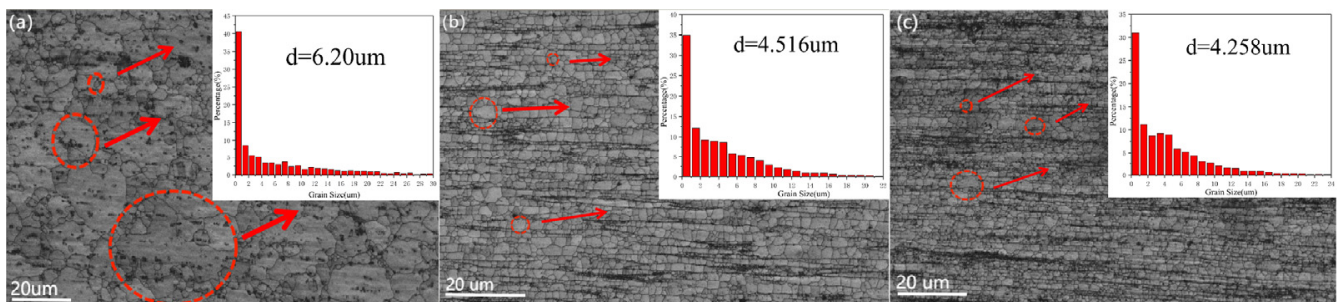


Figure 5. OM images of as-extruded Ti/Mg-3Al-1Zn composites: (a) 0 wt% Ti, (b) 0.5 wt% Ti, (c) 1 wt% Ti.

Figure 6 shows the SEM images of Ti/Mg-3Al-1Zn matrix composites. Figure 6a shows the scanned pattern of the Mg-3Al-1Zn matrix, which has a homogeneous composition, and no other substances were found. In Figure 6b,c, the interface of the composite material is clear, and the strip extrusion trace can be clearly observed. Further magnification of the scanning image can be observed that the gray particles are evenly distributed at the grain boundary. The EDS test results show that the gray particles are composed of Ti elements, which indicates that the nano-Ti reinforcements are uniformly distributed at the grain boundaries of the composite. This phenomenon shows that the addition of nano-Ti particles plays a role in pinning grain boundaries and inhibiting the enhancement of dislocation motion, which is effectively proof that nano-Ti particles play a dispersion-strengthening role on composite materials [59]. In addition, Figure 6c is the scanned image of 1 wt% Ti composite. From the enlarged scanning image, it can be found that there are large gray particles at the grain boundary, which are agglomerated nano-Ti particles. Due

to the increase in the reinforcement content, the nano Ti powder and the matrix powder can not be completely dispersed during the mixing process, so some nano Ti particle agglomerates will be formed in the composite material [60].

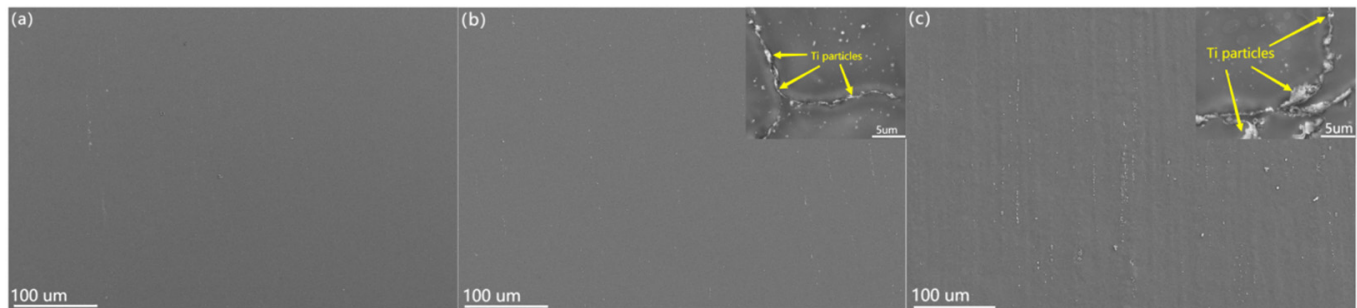


Figure 6. SEM images of as-extruded Ti/Mg-3Al-1Zn composites: (a) 0 wt% Ti, (b) 0.5 wt% Ti, (c) 1 wt% Ti.

Figure 7 illustrates the inverse pole figures (IPF) and pole figures of as-extruded Ti/Mg-3Al-1Zn composites from extrusion direction transverse direction (ED-TD) plane. It shows that the grain sizes of as-extruded composites decrease with the addition of Ti particles, which is accordant with the OM structure in Figure 4. The 0 wt% Ti composites possess the strongest fiber texture intensity 14.2. With the addition of Ti particles, the texture intensity of the composites gradually decreases from 14.2 to 7.58. The decreasing texture is mainly attributed to the DRX aroused by Ti particles [61].

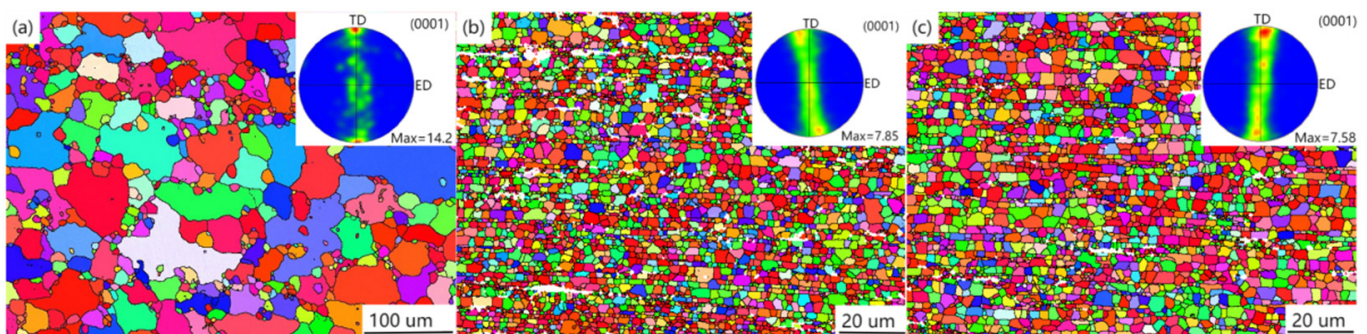


Figure 7. EBSD inverse pole figures and pole figures of as-extruded Ti/Mg-3Al-1Zn composites from ED-TD plane: (a) 0 wt% Ti, (b) 0.5 wt% Ti, (c) 1 wt% Ti.

Figure 8 shows the Schmidt factor diagram for the extruded state (0–0.5) wt% Ti/Mg-3Al-1Zn matrix composite in the TD direction, and the starting probability of the base $\langle a \rangle$, column $\langle a \rangle$, and cone $\langle a \rangle$ sliding system of the composite were analyzed. Figure 8a–c are the Schmidt factor statistics of the Mg-3Al-1Zn matrix composite $\langle a \rangle$ on the base surface, cylinder surface $\langle a \rangle$, and cone surface $\langle a \rangle$. It is not difficult to find that the base plane $\langle a \rangle$ slip system has a higher frequency between 0 and 0.35. It can be inferred that the deformation process of 0 wt% Ti composites is mainly completed through the sliding of the base plane $\langle a \rangle$. The initiation of the base surface $\langle a \rangle$ slip system eventually leads to the formation of the (0001) $\langle 11\text{--}20 \rangle$ texture [62], which is also consistent with the 0 wt% Ti composite having a strong texture on the (0001) surface in Figure 7. In Figure 8b,c, the Schmidt factor of the cylinder $\langle a \rangle$ and cone $\langle a \rangle$ in the TD direction are mainly distributed in the area >0.4 , which reflects that the difficulty of the slip system required to start the deformation in a certain direction of the matrix alloy is unbalanced, resulting in the difference in strength and ductility of the 0 wt% Ti composite [60,63]. As shown in Figure 8d, with the addition of nano Ti, the Schmidt factor of the sliding system of the composite substrate $\langle a \rangle$ is more widely distributed between 0 and 0.5, and the frequency decreases significantly. This phenomenon proves that the strengthening

principle of nano Ti on composites is Orowan strengthening [64]. In addition, the Schmid factor of the slip system on the cylinder $\langle a \rangle$ and the cone $\langle a \rangle$ of the composite also reflects the same situation compared with the matrix material (Figure 8e,f). It reflects the balance of the difficulty of the slip system required to initiate deformation in a certain direction during the plastic deformation process of the composite, so as to achieve a bidirectional improvement of strength and ductility [65–67].

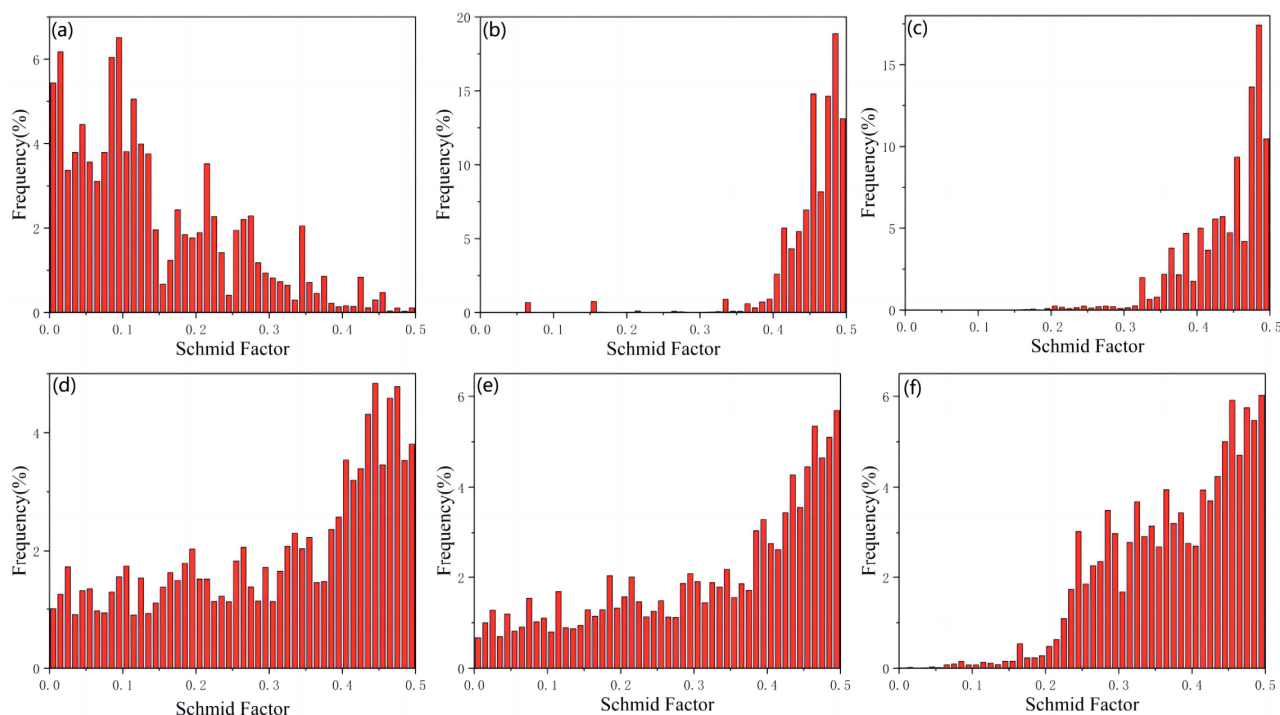


Figure 8. Schmid factor plot patterns of loading in the TD direction: (a) 0 wt% Ti base slide, (b) 0 wt% Ti cylinder slide, (c) 0 wt% Ti pyramidal slide $\langle a \rangle$, (d) 0.5 wt% Ti base slide, (e) 0.5 wt% Ti cylinder slide, (f) 0.5 wt% Ti pyramidal slide $\langle a \rangle$.

Figure 9 shows the engineering stress–strain curves of sintered composites. Table 3 shows the YS (yield strength), UTS (ultimate tensile strength), and ϵ (elongation) values for extruded composites. The results show that with the addition of Ti particles, the YS of the composite increased from 169 MPa to 201 MPa. When Ti particles were added by 0.5 wt%, the UTS of the composite increased from 244 MPa to 304 MPa and the elongation increased from 6.1% to 8.4%. It can be measured that the addition of Ti particles increased the YS, UTS, and ϵ of the composite by 18.9%, 27.7%, and 40%, respectively. The strength and toughness of the 0.5 wt% Ti/Mg-3Al-1Zn matrix composites increased and reached a peak, which also matched the theoretical calculation of the composition. The improvement of the strength of the composites is mainly attributed to the dispersion-strengthening effect of nano-Ti particles. The main reason for the improvement in the strength of the composites is that the addition of nano-Ti particles nails the grain boundaries and inhibits the growth of grains during dynamic recrystallization. The improvement in the elongation of the composites is mainly attributed to the addition of nano-Ti particles, which weakens the texture of the composites and increases the probability of slip and shift start-up. In addition, the strength of the 1 wt% Ti composite is almost the same as that of the 0.5 wt% Ti composite, because the continuous addition of nano-Ti cannot continuously make the grain of the composite finer. On the contrary, the dispersion-strengthening effect of nano-Ti particles is limited by the content of the reinforcement particles, and the increase in the nano-Ti content will lead to a decrease in strength caused by the uneven distribution of the reinforcement particles. The decrease in the ductility of the 1 wt% Ti composite is also due to the agglomeration

of the reinforcement particles at grain boundaries, which is consistent with the results in Figure 6c.

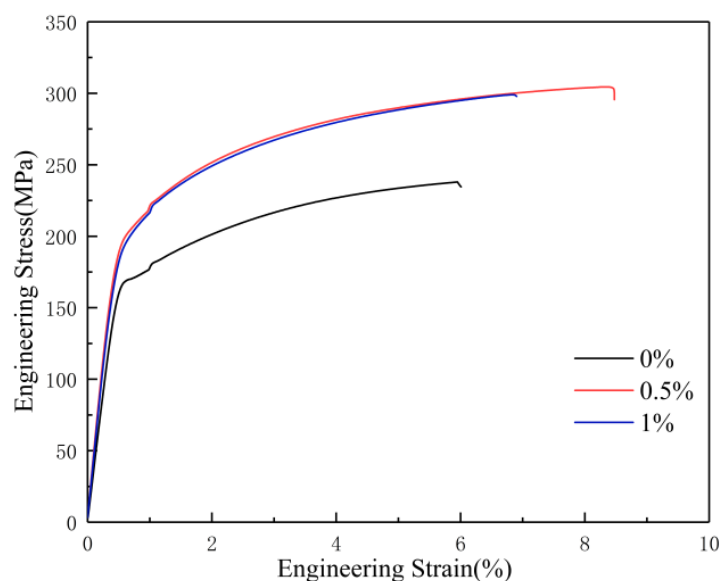


Figure 9. Engineering stress–strain curves of Ti/Mg-3Al-1Zn composites.

Table 4 shows comparative statistics on tensile strength, yield strength, and elongation of the three prepared composites and ASTM B107/B107M-13. As can be seen from the table, the yield strength, tensile strength, and elongation of the 0.5 wt% Ti/Mg-3Al-1Zn matrix composite exceed the peak value of ASTM B107/B107M-13 by 38.6%, 26.7%, and 20%, respectively, which provides options for future light armor materials. Some data of other particle-reinforced Mg-3Al-1Zn matrix composites are also shown in Table 5 [15,68–72]. It is known from Table 5 that SiC-reinforced AZ31 composites have relative high YS and UTS of 380 MPa and 454 MPa, respectively, while their elongation is only 4.75%. However, the graphite grain-reinforced AZ31 composite has a higher elongation of 9.0%, but both their YS and UTS are below 200 MPa. This suggests that it is difficult to bidirectional improve the strength and elongation of particle-reinforced magnesium matrix composites. Compared with other AZ31 composites, the 0.5 wt% Ti/AZ31 material in this study has higher tensile strength and better ductility, and both the strength and ductility of the composite increase, which is also consistent with the discussion in Figure 8 [73,74].

Table 4. Stress–strain statistics of (0–1) wt% Ti/Mg-3Al-1Zn composites and ASTM B107/B107M-13.

	YS (MPa)	UTS (MPa)	ϵ (%)
ASTM B107/B107M-13	145	240	7
0 wt% Ti/Mg-3Al-1Zn	169 ± 1	238 ± 1.1	6.0 ± 0.1
0.5 wt% Ti/Mg-3Al-1Zn	201 ± 1.2	304 ± 2	8.4 ± 0.5
1 wt% Ti/Mg-3Al-1Zn	194 ± 2.2	299 ± 1.5	6.9 ± 1.2

Figure 10 shows the fracture surfaces of the as-extruded composites. In Figure 10a, dimples with coarse sizes and irregular shapes appeared on the fracture surface of the 0 wt% Ti composite. It can be observed that the fracture direction in the dimple is consistent with the tensile direction, reflecting that the stress is more concentrated during deformation. In Figure 10b,c, there are two types of dimples: larger-sized dimples and a large number of small dimples. It is not difficult to observe that spherical Ti particles are adhered to the fine dimples on the surface of the fracture, indicating that the addition of nano-Ti contributes to the formation of small dimples. It is also not difficult to find that the fracture direction is not consistent with the tensile direction, which indicates that the existence of nano-Ti particles

contributes to the stress dispersion during the deformation of composite materials [75]. In addition, the transverse surface can be observed at the fracture, which means that the crack passes through the Ti particles in the tensile test. The Ti particles at the fracture site are not separated from the matrix, indicating that there is a good interfacial bonding between the Ti particles and the Mg matrix. The crack propagation through Ti particles can improve the elongation of the composite [76].

Table 5. Tensile properties of Ti/AZ31 composites and other Mg composites.

Mg Composites	YS (MPa)	UTS (MPa)	ϵ (%)	Fabrication Method
0 wt% Ti	169 ± 1	238 ± 1.1	6.0 ± 0.1	PM + extrusion (this work)
0.5 wt% Ti	201 ± 1.2	304 ± 2	8.4 ± 0.5	
1 wt% Ti	194 ± 2.2	299 ± 1.5	6.9 ± 1.2	
1 wt% Al_2O_3 + AZ31 [70]	186	284	7.52	SPS + extrusion
9.0 wt.% Al/AZ31 [72]	166	198	7.8	Cast + FSP
7.0 vol.% Ti + AZ31 [68]	125	190	6.0	Cast + FSP
7.4 vol.% Graphite + AZ31 [69]	150	190	9.2	Cast + FSP
1 wt% SiC + AZ31 [15]	380	454	4.76	SC

Note: powder metallurgy (PM); friction stir processing (FSP); stir casting (SC).

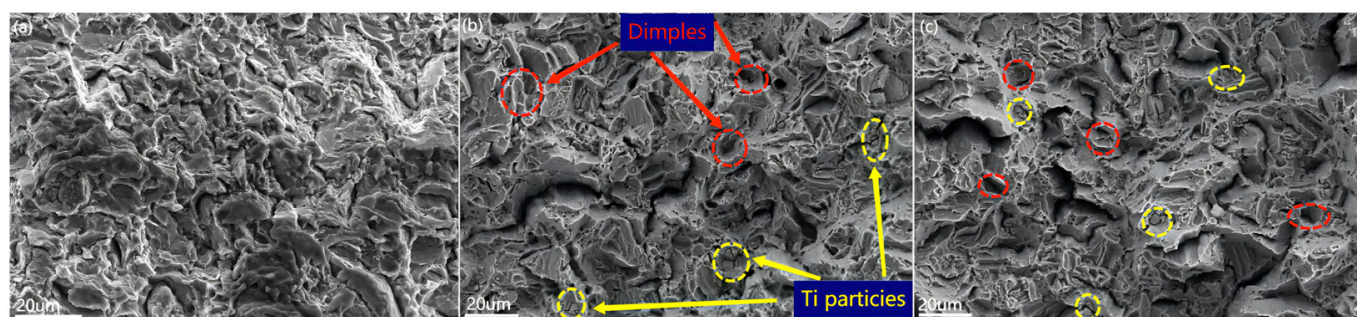


Figure 10. Fracture surfaces of as-extruded Ti/Mg-3Al-1Zn composites: (a) 0 wt% Ti, (b) 0.5 wt% Ti, (c) 1 wt% Ti.

4. Conclusions

In this paper, a novel nano-Ti-reinforced Mg-3Al-1Zn matrix composite suitable for light armor was successfully designed and synthesized, which achieved a bidirectional improvement in strength and ductility. Through XRD, SEM, EBSD, tensile tests, and other characterization or experimental methods, its microstructure and mechanical properties were studied in detail, and the following conclusions could be drawn:

- (1) The addition of nano-Ti particles nailed the grain boundaries, inhibited the grain growth, and significantly reduced the grain size of Ti/Mg-3Al-1Zn composites.
- (2) The YS and UTS of 0.5 wt% Ti/Mg-3Al-1Zn matrix composites reached 201 MPa and 304 MPa, respectively, which exceeded 38.6% and 26.7%, respectively, compared with ASTM B107/B107M-13, and the improvement of strength was mainly due to the nailing of grain boundaries and grain refinement.
- (3) Compared with zero-Ti alloy, the elongation of 0.5 wt% Ti/Mg-3Al-1Zn composite was significantly increased by 40%, which was 20% higher than ASTM B107/B107M-13. The improvement in ductility was the result of the weakening of the texture and the increase in the starting probability of the slip system.
- (4) Compared with micron Ti reinforcement, nano Ti/Mg-3Al-1Zn matrix composites have lower density and better strength and ductility, as well as meeting the requirements of mainstream light armor materials on the market for density and mechanical

properties, which provides new ideas and references for the design and preparation of light armor materials with good mechanical properties.

Author Contributions: Conceptualization, X.C.; Methodology, P.G., S.H., F.Z. and K.Z.; investigation, P.G. and W.T.; writing—original draft, W.T. and P.G.; formal analysis, S.H. and P.G.; resources, Y.Z., T.L., S.H. and W.T. All authors have read and agreed to the published version of the manuscript.

Funding: This work was supported by the National Natural Science Foundation of China (51201107), State Key Laboratory of Advanced Optical Communication Systems and Networks (2018GZKF03007), the manufacturing principle and performance control theory of magnesium/heterogeneous metal composites, a major project of basic and applied basic research in Guangdong Province (2020B0301030006), and Guangdong Academy of Sciences has established a special fund project for the construction of first-class research institutions in China, and a new generation of metal matrix composite interface and performance control and application (2020GDSKXYL-20200101001).

Institutional Review Board Statement: Not applicable.

Informed Consent Statement: Not applicable.

Data Availability Statement: Not applicable.

Conflicts of Interest: The authors declare no conflict of interest.

References

1. Bao, Y.; Gao, X.; Wu, Y.; Sun, M.; Li, G. Research Progress of Armor Protection Materials. *J. Phys. Conf. Ser.* **2021**, *1855*, 012035. [\[CrossRef\]](#)
2. Xu, J.L.; Chen, Y.W.; Wang, R.H.; Li, F.Q.; Liu, A.Y.; Wei, H.Z.; Wang, D.Y.; Li, S.H. Research progress in advanced polymer matrix composites for armor protection systems. *J. Phys. Conf. Ser.* **2020**, *1507*, 06201. [\[CrossRef\]](#)
3. Jiang, Z.G.; Zeng, S.Y.; Shen, Z.Q. Research Progress on Lightweight Ceramic Composite Armor Structure. *Binggong Xuebao/Acta Armamentarii* **2010**, *31*, 603–610.
4. Mukesh, K.; Kant, G.R.; Anand, P. A Review on Fabrication and Characteristics of Metal Matrix Composites Fabricated By Stir Casting. *IOP Conf. Ser. Mater. Sci. Eng.* **2018**, *377*, 012125.
5. Mehara, M.; Goswami, C.; Kumar, S.R.; Singh, G.; Wagdre, M.K. Performance evaluation of advanced armor materials. *Mater. Today Proc.* **2021**, *47*, 6039–6042. [\[CrossRef\]](#)
6. Song, J.F.; She, J.; Chen, D.L.; Pan, F.S. Latest research advances on magnesium and magnesium alloys worldwide. *J. Magnes. Alloy.* **2020**, *8*, 1–41. [\[CrossRef\]](#)
7. Ma, G.; Xiao, H.; Ye, J.; He, Y. Research status and development of magnesium matrix composites. *Mater. Sci. Technol.* **2020**, *36*, 645–653. [\[CrossRef\]](#)
8. Singh, N.; Belokar, R.M. Tribological behavior of aluminum and magnesium-based hybrid metal matrix composites: A state-of-art review. *Mater. Today Proc.* **2021**, *44*, 460–466. [\[CrossRef\]](#)
9. Salasel, A.R.; Abbasi, A.; Barri, N.; Mirzadeh, H.; Emamy, M.; Malekan, M. Effect of Si and Ni on microstructure and mechanical properties of in-situ magnesium-based composites in the as-cast and extruded conditions. *Mater. Chem. Phys.* **2019**, *232*, 305–310. [\[CrossRef\]](#)
10. Wu, B.; Li, J.B.; Ye, J.L.; Tan, J.; Liu, L.Z.; Song, J.F.; Chen, X.H.; Pan, F.S. Work hardening behavior of Ti particle reinforced AZ91 composite prepared by spark plasma sintering. *Vacuum* **2021**, *183*, 109833. [\[CrossRef\]](#)
11. Rubtsov, V.; Chumaevskii, A.; Gusarova, A.; Knyazhev, E.; Gurianov, D.; Zykova, A.; Kalashnikova, T.; Cheremnov, A.; Savchenko, N.; Vorontsov, A.; et al. Macro- and Microstructure of In Situ Composites Prepared by Friction Stir Processing of AA5056 Admixed with Copper Powders. *Materials* **2023**, *16*, 1070. [\[CrossRef\]](#) [\[PubMed\]](#)
12. Saikrupa, C.; Reddy GC, M.; Venkatesh, S. Aluminium metal matrix composites and effect of reinforcements—A Review. *IOP Conf. Ser. Mater. Sci. Eng.* **2021**, *1057*, 012098. [\[CrossRef\]](#)
13. Vinayagam, M.; Ravichandran, M. Influence of AlN particles on microstructure, mechanical and tribological behaviour in AA6351 aluminum alloy. *Mater. Res. Express* **2019**, *6*, 106557.
14. Ali, A.N.; Huang, S.J. Experimental investigations of effects of SiC contents and severe plastic deformation on the microstructure and mechanical properties of SiCp/AZ61 magnesium metal matrix composites. *J. Mater. Process. Technol.* **2019**, *272*, 28–39.
15. Ballóková, B.; Falat, L.; Puchý, V.; Molčanová, Z.; Besterci, M.; Džunda, R.; Abbas, A.; Huang, S.-J. The Influence of Laser Surface Remelting on the Tribological Behavior of the ECAP-Processed AZ61 Mg Alloy and AZ61-Al₂O₃ Metal Matrix Composite. *Materials* **2020**, *13*, 2688. [\[CrossRef\]](#) [\[PubMed\]](#)
16. Güleriyüz, L.F.; Ozan, S.; İpek, R.; Uzunsoy, D. Production of B4Cp reinforced magnesium metal matrix composites by powder metallurgy. *Usak Univ. J. Mater. Sci.* **2014**, *2012*, 51–58.
17. Yao, J.; Li, W.; Zhang, L.; Wang, F.; Xue, M.; Jiang, H.; Lu, J. Wear Mechanism for In Situ TiC Particle Reinforced AZ91 Magnesium Matrix Composites. *Tribol. Lett.* **2010**, *38*, 253–257. [\[CrossRef\]](#)

18. Ali, Y.; Qiu, D.; Jiang, B.; Pan, F.; Zhang, M.-X. Current research progress in grain refinement of cast magnesium alloys: A review article. *J. Alloys Compd.* **2015**, *619*, 639–651. [\[CrossRef\]](#)
19. Wu, H.; Shan, Z.; Fan, J.; Zhang, Q.; Deng, K.; Wu, Y.; Li, W.; Dong, H.; Xu, B. Microstructure and mechanical properties of SiCp/AZ91 composite processed with extrusion and EPT. *Mater. Sci. Technol.* **2021**, *37*, 269–279. [\[CrossRef\]](#)
20. Xiao, P.; Gao, Y.; Yang, C.; Liu, Z.; Li, Y.; Xu, F. Microstructure, mechanical properties and strengthening mechanisms of Mg matrix composites reinforced with in situ nanosized TiB₂ particles. *Mater. Sci. Eng. A-Struct. Mater. Prop. Microstruct. Process.* **2018**, *710*, 251–259. [\[CrossRef\]](#)
21. Habibnejad-Korayem, M.; Mahmudi, R.; Poole, W.J. Enhanced properties of Mg-based nano-composites reinforced with Al₂O₃ nano-particles. *Mater. Sci. Eng. A* **2009**, *519*, 198–203. [\[CrossRef\]](#)
22. Wang, J.J.; Guo, J.H.; Chen, L.Q. TiC/AZ91D composites fabricated by in situ reactive infiltration process and its tensile deformation. *J. China Nonferrous Met. Assoc.* **2006**, *16*, 5. [\[CrossRef\]](#)
23. Ye, J.; Li, J.; Luo, H.; Tan, J.; Chen, X.; Feng, B.; Zheng, K.; Pan, F. Effect of micron-Ti particles on microstructure and mechanical properties of Mg–3Al–1Zn based composites. *Mater. Sci. Eng. A* **2022**, *833*, 142526. [\[CrossRef\]](#)
24. Zhou, M.; Qu, X.; Ren, L.; Fan, L.; Zhang, Y.; Guo, Y.; Quan, G.; Tang, Q.; Liu, B.; Sun, H. The Effects of Carbon Nanotubes on the Mechanical and Wear Properties of AZ31 Alloy. *Materials* **2017**, *10*, 1385. [\[CrossRef\]](#)
25. Feng, Y.; Chen, C.; Wang, R.; Wang, X. Ni particles enhance the microorganization and mechanical properties of AZ 61 composites. *Powder Metall. Mater. Sci. Eng.* **2018**, *23*, 562–568.
26. Wong, W.; Gupta, M. Development of Mg/Cu nanocomposites using microwave assisted rapid sintering. *Compos. Sci. Technol.* **2007**, *67*, 1541–1552. [\[CrossRef\]](#)
27. Chiu, C.; Chang, H.-H. Al_{0.5}CoCrFeNi₂ High Entropy Alloy Particle Reinforced AZ91 Magnesium Alloy-Based Composite Processed by Spark Plasma Sintering. *Materials* **2021**, *14*, 6520. [\[CrossRef\]](#)
28. Ho, K.F.; Gupta, M.; Srivatsan, T.S. The mechanical behavior of magnesium alloy AZ91 reinforced with fine copper particulates. *Mater. Sci. Eng. A* **2004**, *369*, 302–308. [\[CrossRef\]](#)
29. Kwasniak, P.; Wrobel, J.S.; Garbacz, H. Origin of low Young modulus of multicomponent, biomedical Ti alloys—Seeking optimal elastic properties through a first principles investigation. *J. Mech. Behav. Biomed. Mater.* **2018**, *88*, 352–361. [\[CrossRef\]](#)
30. Dieringa, H. Properties of magnesium alloys reinforced with nanoparticles and carbon nanotubes: A review. *J. Mater. Sci.* **2011**, *46*, 289–306. [\[CrossRef\]](#)
31. Moslem, T.; Morteza, A. A novel two-step method for producing Al/Cu functionally graded metal matrix composite. *J. Alloys Compd.* **2022**, *911*, 165078.
32. Shen, M.J.; Zhang, M.F.; Ying, W.F. Processing, microstructure and mechanical properties of bimodal size SiCp reinforced AZ31B magnesium matrix composites. *J. Magnes. Alloy.* **2015**, *3*, 162–167. [\[CrossRef\]](#)
33. Moslem, T.; Morteza, A. Thermal and wear properties of Al/Cu functionally graded metal matrix composite produced by severe plastic deformation method. *J. Manuf. Process.* **2023**, *85*, 515–526.
34. Zheng, M.Y.; Wu, K.; Yao, C.K. Effect of interfacial reaction on mechanical behavior of SiCw/AZ91 magnesium matrix composites. *Mater. Sci. Eng. A* **2001**, *318*, 50–56. [\[CrossRef\]](#)
35. Zhao, C.; Qi, Z.; Wang, X.; Zhang, Z. Fabrication and characterization of monolithic nanoporous copper through chemical dealloying of Mg–Cu alloys. *Corros. Sci.* **2009**, *51*, 2120–2125. [\[CrossRef\]](#)
36. Hu, X.S.; Zhang, Y.K.; Zheng, M.Y.; Wu, K. A study of damping capacities in pure Mg and Mg–Ni alloys. *Scr. Mater.* **2005**, *52*, 1141–1145. [\[CrossRef\]](#)
37. Edalati, K.; Emami, H.; Staykov, A.; Smith, D.J.; Akiba, E.; Horita, Z. Formation of metastable phases in magnesium–titanium system by high-pressure torsion and their hydrogen storage performance. *Acta Mater.* **2015**, *99*, 150–156. [\[CrossRef\]](#)
38. Umeda, J.; Kawakami, M.; Kondoh, K.; Ayman, E.L.S.; Imai, H. Microstructural and mechanical properties of titanium particulate reinforced magnesium composite materials. *Mater. Chem. Phys.* **2010**, *123*, 649–657. [\[CrossRef\]](#)
39. Braszczyńska-Malik, K.N.; Przełoczyńska, E. Analyses of AM50-TiP metal-metal composite microstructure. *J. Alloys Compd.* **2018**, *731*, 1181–1187. [\[CrossRef\]](#)
40. Kondoh, K.; Kawakami, M.; Imai, H.; Umeda, J.; Fujii, H. Wettability of pure Ti by molten pure Mg droplets. *Acta Mater.* **2010**, *58*, 606–614. [\[CrossRef\]](#)
41. Kitazono, K.; Komatsu, S.; Kataoka, Y. Mechanical properties of titanium particles dispersed magnesium matrix composite produced through accumulative diffusion bonding process. *Mater. Trans.* **2011**, *52*, 155–158. [\[CrossRef\]](#)
42. Wang, S.; Huang, L.; Zhang, R.; Liu, B.; Cui, X.; Geng, L.; Peng, H. Enhancing ductility of titanium matrix composites by multimodal α -grains. *Scr. Mater.* **2019**, *170*, 161–165. [\[CrossRef\]](#)
43. Niu, H.Z.; Zhang, H.R.; Sun, Q.Q.; Zhang, D.L. Breaking through the strengthductility trade-off dilemma in powder metallurgy Ti–6Al–4V titanium alloy. *Mater. Sci. Eng. A* **2019**, *754*, 361–369. [\[CrossRef\]](#)
44. Dinaharan, I.; Zhang, S.; Chen, G.; Shi, Q. Development of titanium particulate reinforced AZ31 magnesium matrix composites via friction stir processing. *J. Alloys Compd.* **2020**, *820*, 153071. [\[CrossRef\]](#)
45. Dinaharan, I.; Zhang, S.; Chen, G.; Shi, Q. Titanium particulate reinforced AZ31 magnesium matrix composites with improved ductility prepared using friction stir processing. *Mater. Sci. Eng. A* **2020**, *772*, 138793. [\[CrossRef\]](#)
46. Sankaranarayanan, S.; Jayalakshmi, S.; Gupta, M. Effect of individual and combined addition of micro/nano-sized metallic elements on the microstructure and mechanical properties of pure Mg. *Mater. Des.* **2012**, *37*, 274–284. [\[CrossRef\]](#)

47. Park, H.K.; Jung, J.; Kim, H.S. Three-dimensional microstructure modeling of particulate composites using statistical synthetic structure and its thermo-mechanical finite element analysis. *Comput. Mater. Sci.* **2017**, *126*, 265–271. [\[CrossRef\]](#)
48. Yuan, Z.W.; Li, F.G.; Xue, F.M.; He, M.; Hussain, M.Z. Analysis of the stress states and interface damage in a particle reinforced composite based on a micromodel using cohesive elements. *Mater. Sci. Eng. A* **2014**, *589*, 288–302. [\[CrossRef\]](#)
49. Deng, K.K.; Wang, X.J.; Wu, Y.W.; Hu, X.S.; Wu, K.; Gan, W.M. Effect of particle size on microstructure and mechanical properties of SiCp/AZ91 magnesium matrix composite. *Mater. Sci. Eng. A* **2012**, *543*, 158–163. [\[CrossRef\]](#)
50. Zhang, F.; Huang, Y.; Hwang, K.C.; Qu, S.; Liu, C. A three-dimensional strain gradient ductility analysis of particle size effect in composite materials. *Mater. Manuf. Process.* **2007**, *22*, 140–148. [\[CrossRef\]](#)
51. Cao, D.; Duan, Q.; Li, S.; Zhong, Y.; Hu, H. Effects of thermal residual stresses and thermal-induced geometrically necessary dislocations on size-dependent strengthening of particle-reinforced MMCs. *Compos. Struct.* **2018**, *200*, 290–297. [\[CrossRef\]](#)
52. Chen, Y.; Yao, Y.; Han, S.; Feng, X.; Luo, T.; Zheng, K. Study on Microstructure and Mechanical Properties of TC4/AZ31 Magnesium Matrix Nanocomposites. *Materials* **2023**, *16*, 1139. [\[CrossRef\]](#)
53. Yu, H.; Zhou, H.; Sun, Y.; Ren, L.; Wan, Z.; Hu, L. Microstructures and mechanical properties of ultrafine-grained Ti/AZ31 magnesium matrix composite prepared by powder metallurgy. *Adv. Powder Technol.* **2018**, *29*, 3241–3249. [\[CrossRef\]](#)
54. Rashad, M.; Pan, F.; Tang, A.; Lu, Y.; Asif, M.; Hussain, S.; She, J.; Gou, J.; Mao, J. Effect of graphene nanoplatelets (GNPs) addition on strength and ductility of magnesium/titanium alloys. *J. Magnes. Alloy.* **2013**, *1*, 242–248. [\[CrossRef\]](#)
55. Tadros, T.F. *Dispersion of Powders*; Wiley-VCH: Weinheim, Germany, 2012.
56. Lider, V.V. X-ray diffraction methods for diagnostics of surface and nanolayers of crystalline structures (review). *Inorg. Mater.* **2014**, *50*, 1459–1469. [\[CrossRef\]](#)
57. Xin, R.L.; Wang, B.S.; Chen, X.P.; Huang, G.J.; Liu, Q. EBSD analysis of microstructure and texture in deformed magnesium alloy. *J. Chin. Electron Microsc. Soc.* **2008**, *27*, 4.
58. Yang, B.; Wang, Y.; Gao, M.; Wang, C.; Guan, R. Microstructural evolution and strengthening mechanism of Al-Mg alloys with fine grains processed by accumulative continuous extrusion forming. *J. Mater. Sci. Technol.* **2022**, *128*, 195–204. [\[CrossRef\]](#)
59. Tong, W.; An, Y.; Bao, C.; Fang, D.; Wang, M.; Yi, J. Improving mechanical properties of copper composite by interconnected MoO₂ quantum dots. *Mater. Sci. Eng. A* **2022**, *848*, 143365. [\[CrossRef\]](#)
60. Tang, C.; Chen, J.; Ma, X.; Liu, W.; Xie, H.; Li, M.; Liu, X. Effects of extrusion speed on the formation of bimodal-grained structure and mechanical properties of a Mg-Gd-based alloy. *Mater. Charact.* **2022**, *189*, 111952. [\[CrossRef\]](#)
61. Novak, S.; Lorenzetti, M.; Drame, A.; Vidmar, J.; Ščančar, J.; Filipič, M. Diversity of TiO₂ nanopowders' characteristics relevant to toxicity testing. *Journal of nanoparticle research: An interdisciplinary forum for nanoscale science and technology. J. Nanoparticle Res.* **2016**, *18*, 130. [\[CrossRef\]](#)
62. Li, W.; Chen, Z.; Liu, J.; Wang, Q.; Sui, G. Effect of texture on anisotropy at 600 °C in a near- α titanium alloy Ti60plate. *Mater. Sci. Eng. A* **2017**, *688*, 322–329. [\[CrossRef\]](#)
63. Germain, L.; Gey, N.; Humbert, M.; Vo, P.; Jahazi, M.; Bocher, P. Texture heterogeneities induced by subtransus processing of near α titanium alloys. *Acta Mater.* **2008**, *56*, 4298–4308. [\[CrossRef\]](#)
64. Ye, X.P.; Li, Y.L.; Weng, J.D.; Cai, L.C.; Liu, C.L. Research Status on Strengthening Mechanism of Particle-reinforced Metal Matrix Composites. *Cailiao Gongcheng/J. Mater. Eng.* **2018**, *46*, 28–37.
65. Uta, E.; Gey, N.; Bocher, P.; Humbert, M. Texture heterogeneities in α p/ α s titanium forging analysed by EBSD-Relation to fatigue crack propagation. *J. Microsc.* **2009**, *233*, 451–459. [\[CrossRef\]](#)
66. Yan, Z.; Wang, D.; He, X. Deformation behaviors and cyclic strength assessment of AZ31B magnesium alloy based on steady ratcheting effect. *Mater. Sci. Eng. A* **2018**, *723*, 212–220. [\[CrossRef\]](#)
67. Won, J.W.; Kim, D.; Hong, S.-G.; Lee, C.S. Anisotropy in twinning characteristics and texture evolution of rolling textured high purity alpha phase titanium. *J. Alloys Compd.* **2016**, *683*, 92–99. [\[CrossRef\]](#)
68. Gey, N.; Bocher, E.; Germain, L.; Humbert, M. Texture and microtexture variations in a near- α titanium forged disk of bimodal microstructure. *Acta Mater.* **2012**, *60*, 2647–2655. [\[CrossRef\]](#)
69. Vahedi, F.; Zarei-Hanzaki, A.; Salandari-Rabori, A.; Abedi, H.R.; Razaghian, A.; Minarik, P. Microstructural evolution and mechanical properties of thermomechanically processed AZ31 magnesium alloy reinforced by micro-graphite and nano-graphene particles. *J. Alloys Compd.* **2020**, *815*, 152231. [\[CrossRef\]](#)
70. Yu, H.; Sun, Y.; Wan, Z.; Zhou, H.; Hu, L. Nanocrystalline Ti/AZ61 magnesium matrix composite: Evolution of microstructure and mechanical property during annealing treatment. *J. Alloys Compd.* **2018**, *741*, 231–239. [\[CrossRef\]](#)
71. Braszczynska-Malik, K.N.; Przełoczyńska, E. The influence of Ti particles on microstructure and mechanical properties of Mg-5Al-5RE matrix alloy composite. *J. Alloys Compd.* **2017**, *728*, 600–606. [\[CrossRef\]](#)
72. Sahu, P.K.; Das, J.; Chen, G.; Liu, Q.; Pal, S.; Zeng, S.; Shi, Q. Friction stir selective alloying of different Al% particulate reinforced to AZ31 Mg for enhanced mechanical and metallurgical properties. *Mater. Sci. Eng. A* **2019**, *774*, 138889. [\[CrossRef\]](#)
73. Yuan, Q.; Zhou, G.; Liao, L.; Liu, Y.; Luo, L. Interfacial structure in AZ91 alloy composites reinforced by graphene nanosheets. *Carbon* **2018**, *127*, 177–186. [\[CrossRef\]](#)
74. Bočan, J.; Maňák, J.; Jäger, A. Nanomechanical analysis of AZ31 magnesium alloy and pure magnesium correlated with crystallographic orientation. *Mater. Sci. Eng. A* **2015**, *644*, 121–128. [\[CrossRef\]](#)

75. Modina, I.M.; Dyakonov, G.S.; Stotskiy, A.G.; Yakovleva, T.V.; Semenova, I.P. Effect of the Texture of the Ultrafine-Grained Ti-6Al-4V Titanium Alloy on Impact Toughness. *Materials* **2023**, *16*, 1318. [[CrossRef](#)]
76. P'erez, P.; Garces, G.; Adeva, P. Mechanical properties of a Mg–10 (vol.%)Ti composite. *Compos. Sci. Technol.* **2004**, *64*, 145–151. [[CrossRef](#)]

Disclaimer/Publisher's Note: The statements, opinions and data contained in all publications are solely those of the individual author(s) and contributor(s) and not of MDPI and/or the editor(s). MDPI and/or the editor(s) disclaim responsibility for any injury to people or property resulting from any ideas, methods, instructions or products referred to in the content.